Materials & Design 232 (2023) 112175

Contents lists available at ScienceDirect

Materials & Design

journal homepage: www.elsevier.com/locate/matdes

On the consequences of intrinsic and extrinsic size effects on the mechanical response of nanoporous Au

Yijuan Wu [a], Jürgen Markmann [a,b,*], Erica T. Lilleodden [a,c]

[a] Helmholtz-Zentrum Hereon, Institute of Materials Mechanics, 21502 Geesthacht, Germany
[b] Hamburg University of Technology, Institute of Materials Physics and Technology, 21073 Hamburg, Germany
[c] Fraunhofer Institute for Microstructure of Materials and Systems, 06120 Halle, Germany

ARTICLE INFO

Keywords:
Microcompression testing
Nanoporus gold
Microstructural size effect
Sample size effect

ABSTRACT

In this study, the consequence of intrinsic and extrinsic size effects on mechanical responses of nanoporous gold is investigated via microcompression testing. By varying the micropillar diameter (D) between 1 μm and 20 μm and the ligament size (L), 50 nm and 350 nm, a critical ratio ($\alpha = D/L = 20$) was found, above which the test structure can be considered a representative volume element, resulting in identical mechanical response and uniform deformation. Below that value, both flow stress and elastic modulus decrease with decreasing pillar diameter, as evidenced for a measurement series with a fixed ligament size of 350 nm where the flow stress decreased by more than 50% (from approximately 5 to 2.5 MPa) and the elastic modulus was reduced from approximately 0.5 GPa to almost zero. Stochastic behavior along with non-uniform deformation and failure is observed for $\alpha < 10$, suggesting that the size of the load-bearing units in this material is about 10 times the corresponding ligament size.

1. Introduction

Size effects in the mechanical behavior of metals have received much attention over the past few decades, where the ability to test micro- and nano-scale objects has revealed mechanistic changes in deformation resulting in size dependent strength, as well as the influence of high surface to volume ratios. While many studies yield fundamental insight such as "smaller-is-stronger", the consequences of such size effects are not always so evident. The existence of both intrinsic and extrinsic size effects can complicate attempts to find scaling laws to predict the behavior. A prominent example is hierarchically structured nanoporous gold (NPG), a bicontinuous network structure across two structural length scales [1,2]. Here, intermittent dealloying and coarsening leads to a bicontinuous network structure where the interconnected ligaments are themselves nanoporous. As was shown by Volkert *et al.* in 2006 [3], the strength of NPG can be increased significantly by decreasing the microstrucutural length scale until the theoretical shear strength is reached in ligaments, while no size effect was observed for varying deformation volumes. However, the volumes tested all remained large as compared to the ligament or pore size. Given that the ligament size in hierarchical NPG may be tailored such that only several nanopores span across it, the potential for finite size effects may have very important consequences on the overall mechanical response [2] – there may be a critical limit to the usual smaller-is-stronger paradigm typically invoked in the literature [4–6]. In order to develop design strategies for materials systems with multiple microstructural size levels, this interplay of the different size effects needs further exploration.

A geometrical size effect has been observed in cellular materials with millimeter cell size [7,8], such as Aluminum foams with stochastic honeycomb structure [9,10] and reticulated vitreous carbon consisting of relatively isotropic open cells [11], when the deformation size, i.e. flat punch diameter of the indenter or the sample size itself, is the order of the cell size. Nanoindentation experiments showed an increase of mechanical strength and stiffness as the ratio of flat punch diameter to cell size decreased, resulting from edge effects at the contact perimeter. At the same time, the opposite is observed for compression results where the strength and elastic modulus decreased with decreasing ratio of sample size to cell size, due to the decreased constraints at the free surface, making the surface cells more compliant; together with the increased area fraction of cut cell walls at the boundary that remain stress-free.

In the case of NPG with its self-organized bicontinuous network structure, the relative density still is the main parameter determining mechanical properties [12–14]. In recent studies, it was found that,

* Corresponding author at: Helmholtz-Zentrum Hereon, Institute of Materials Mechanics, 21502 Geesthacht, Germany.
E-mail address: juergen.markmann@hereon.de (J. Markmann).

https://doi.org/10.1016/j.matdes.2023.112175
Received 10 May 2023; Received in revised form 4 July 2023; Accepted 17 July 2023
Available online 18 July 2023

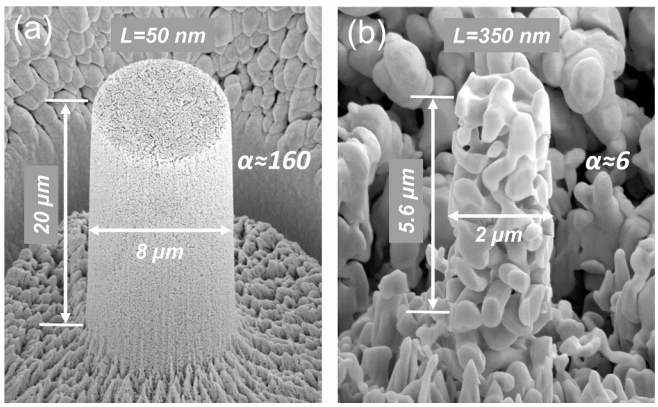

Fig. 1. SEM images of pillars with different ratio α of middle diameter *(D)* to ligament size *(L)*. (a) $D = 8$ μm, $H = 20$ μm, $L \approx 50$ nm, $\alpha = D/L = 160$. (b) $D = 2$ μm, $H = 5.5$ μm, $L = 350$ nm, $\alpha = D/L = 6$.

besides the density, the structural geometry, such as ligament size and connectivity, also have significant impact on the strength and stiffness [15–20].

The effect of geometric size on porous materials, which is important for the above described reasons, has not been systematically investigated, especially if there only are few building units in the volume involved. In this study, a set of micro-compression tests is carried out on NPG pillars with varying structural size (intrinsic size) and deformation volume (extrinsic size) using a nanoindenter equipped with a flat punch, aiming at addressing the consequence of these intrinsic and extrinsic size effects as well as their relation to each other on the mechanical behavior.

2. Experiment

Bulk NPG specimens used for the current study were generated by dealloying an $Ag_{75}Au_{25}$ alloy (atomic ratio), the synthesis process of which is similar to that described in [21]. Briefly, $Ag_{75}Au_{25}$ alloy ingots were fabricated by arc melting (MAM-1, Edmund Bühler) corresponding amounts of gold and silver wires (Sigma-Aldrich, purity 99.99%). After homogenization at 850 °C for 120 h in vacuum ($<10^{-6}$ mbar, custom made setup using a RHF1600, Carbolite tube furnace), cylinders of 1 mm in diameter and 2 mm in height were obtained by wire drawing and cutting. Prior to electrochemical dealloying, samples were mechanically polished and annealed at 800 °C for 1 h in Ar atmosphere (Ar 5.0, infrared furnace behr IRF 10, behr Labor Technik) in order to relieve residual stresses, which probably have remained after the shaping process. After that, silver was dissolved at room temperature in 1 M $HClO_4$,

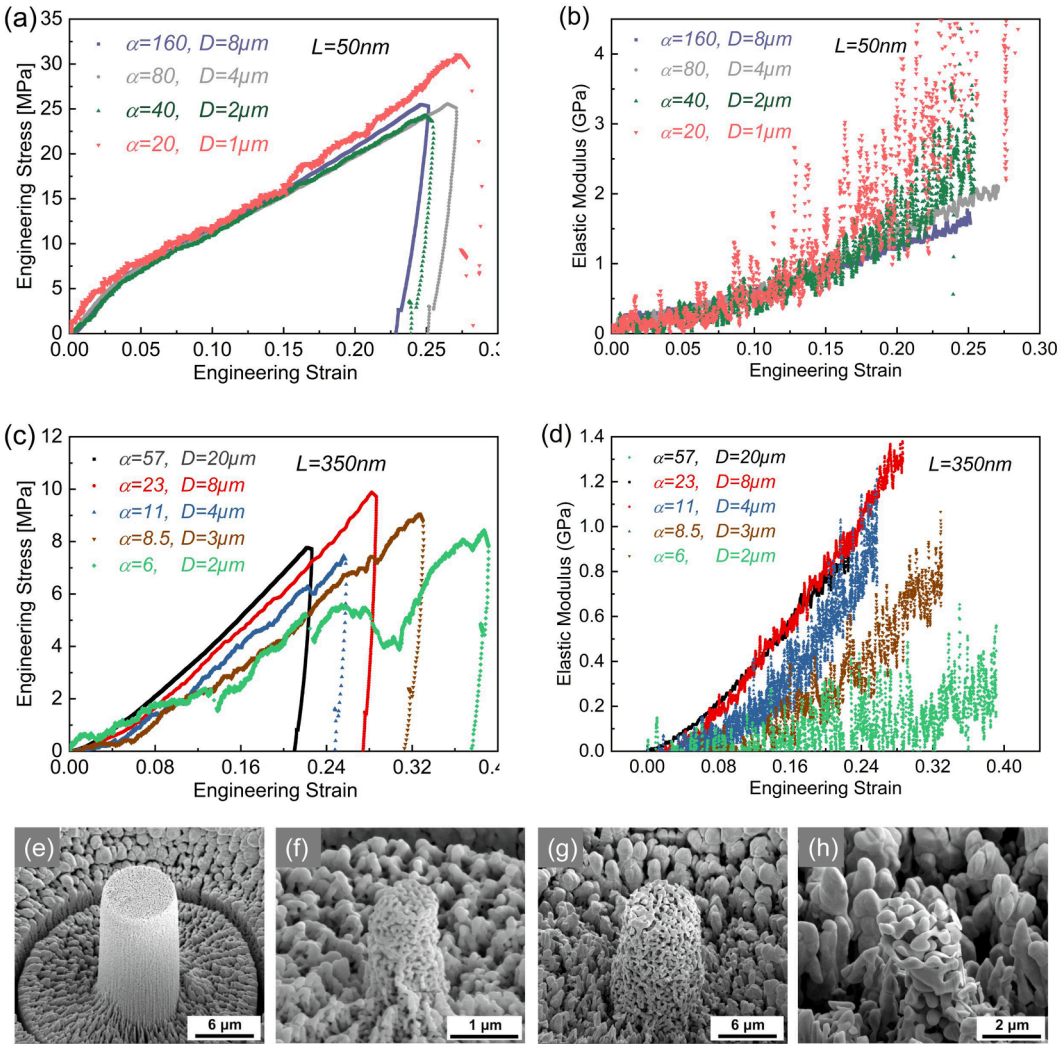

Fig. 2. Compression results of NPG pillars with varying ratios ($\alpha = D/L$) of pillar diameter (D) to ligament size (L). (a) Engineering stress–strain curves and (b) elastic modulus of pillar with $L = 50$ nm, where α ranging from 160 to 20. (c) Engineering stress–strain curves and (d) elastic modulus of pillar with $L = 350$ nm, where α ranging from 57 to 6. (e)-(h) SEM images of pillars with (e) $\alpha = 160$, (f) $\alpha = 20$, (g) $\alpha = 23$ and (h) $\alpha = 6$ after compression.

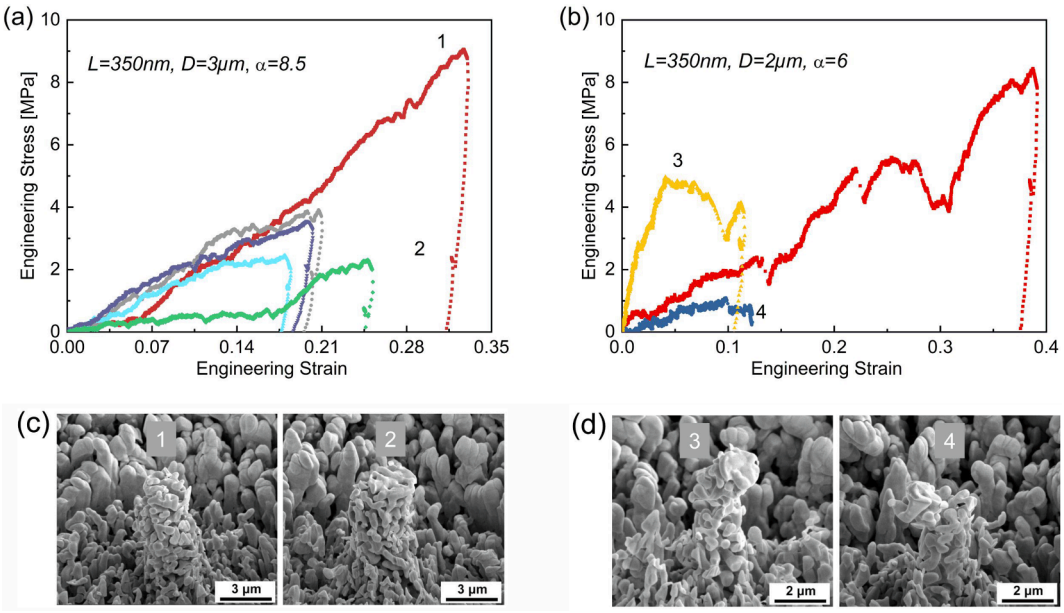

Fig. 3. Compression results of NPG pillars with low ($\alpha = D/L$) of pillar diameter (D) to ligament size ($L = 350$ nm). Engineering stress–strain curves of pillars with (a) $\alpha = 8.5$ ($D = 3$ μm) and (b) $\alpha = 6$ ($D = 2$ μm). SEM images of pillars with (c) $\alpha = 8.5$ and (d) $\alpha = 6$ after compression.

diluted from conc. acid (60% p.a. grade, Merck, Alfa Aesar) and ultrapure water (Ultra Clear TWF UV TM, Siemens), with application of an electrochemical potential of 1.25 V, versus Standard Hydrogen Electrode (SHE, Gaskatel) until the current declined below 10 μA. Subsequently, the residual Ag was further removed from as-dealloyed samples by applying 15 potential cycles between 0 and 1.5 V (scan rate, 5 mV/s) in a fresh 1 M $HClO_4$ solution. Finally, NPG samples were repeatedly rinsed and infiltrated in ultrapure water for 24 h, then dried in air.

The ligament size of NPG prepared by the method described above is around 35 nm, as measured by Scanning Electron Microscopy (SEM, see below) inspection. Samples with coarser ligament sizes of 50 nm and 350 nm were obtained by post-annealing at 300 °C for 12 min and 500 °C for 1 h in air, respectively. Afterwards, bulk NPG samples with different ligament size are transferred to SEM stubs for micropillar fabrication. Pillars with a middle-diameter ranging from 20 to 1 μm, and with an aspect ratio of ca. 3:1 (height to middle-diameter) were produced on the (prior to dealloying) polished surface of NPG cylinders using Focused Ion Beam (FIB) machining installed on a FEI Nanolab 200 SEM. Since each pillar has two varying length-scales, ligament size (L) and pillar diameter (D), the ratio $\alpha = D/L$ (a relative value describing the ratio of the geometric to microstructure length-scale) is used here as a characteristic parameter to couple these two length-scales. The total range of α used in the present study is from 6 to 160, and the SEM images of pillars with maximum and minimum α are shown in Fig. 1. Both pillars show a homogeneous bicontinuous structure and no significant deposition caused by the FIB cutting is observed. Apparently, the number of ligaments involved in the pillar decreases with decreasing α, implying that the number of interconnected ligaments which provide structural support and contribute to the mechanical behavior decreases as α decreases too.

A set of microcompression tests were conducted on pillars with varying α at room temperature using a Nanoindenter (MTS XP) outfitted with a flat punch tip made from diamond. During testing, pillars were compressed at a fixed strain rate of 0.001/s to the maximum displacement, after which they underwent a load-holding period of 10 s prior to unloading. The load–displacement curves were recorded directly by the instrument. With the Continuous Stiffness Measurement (CSM) option applied, the contact stiffness of the sample can be measured continuously by imposing an oscillation signal with an amplitude of 2 nm and a fixed frequency of 45 Hz, which can be used for simultaneous determination of the change in elastic modulus of the pillars during testing. After testing, the raw displacement of the pillar was corrected by subtracting the contributions from the load-frame of the machine and the substrate material below the tested pillar. The contribution of the substrate material, where the pillar acts like a flat punch pushing into the bulk nanoporous gold during compression, can be obtained using the Sneddon correction [22]. The engineering stress–strain curves were calculated from the corrected load–displacement curves, using the initial middle-diameter and height of the corresponding pillar as geometrical descriptors.

3. Results

Results from microcompression of pillars with varying ratio ($\alpha = D/L$) of diameter (D) to ligament size (L) are shown in Fig. 2 and Fig. 3. Each aspect ratio, α, was tested at least three times. If the stress–strain curves of these three or more samples were largely identical, one curve was selected to be representative and shown in Fig. 2. Fig. 3 shows stress–strain curves of samples with lower α which do not coincide. The engineering stress–strain curves exhibited in Fig. 2(a), where the pillar diameter (D) ranging from 8 to 1 μm is sufficiently larger than the ligament size ($L = 50$ nm), are identical. They reveal no effect of deformation length-scale on the magnitude of the stress in the plastic regime when α of pillar varies from 160 down to 20, consistent with the corresponding results in [3]. The transition from elastic to plastic deformation can be observed as a change of slope in the stress–strain curves. With the CSM mode, the elastic modulus as a function of engineering strain was obtained. These results are shown in Fig. 2(b). The stiffness increases considerably with increasing strain during deformation, due to the densification of the porous structure. However, it is insensitive to the variation of α, in agreement with the trend in the flow stress; both modulus and flow stress are not dependent on α for a given microstructure. The SEM images of pillars with $\alpha = 160$ ($D = 8$ μm) and $\alpha = 20$ ($D = 1$ μm) after compression, as presented in Fig. 2 (e) and (f), respectively, confirm that those pillars experience a uniform deformation.

In contrast, the corresponding microcompression results of pillars with larger ligament size ($L = 350$ nm), shown in Fig. 2 (c) and (d), where the pillar diameter changes from 20 to 2 μm and the corresponding α ranges from 57 to 6, exhibit differences in mechanical

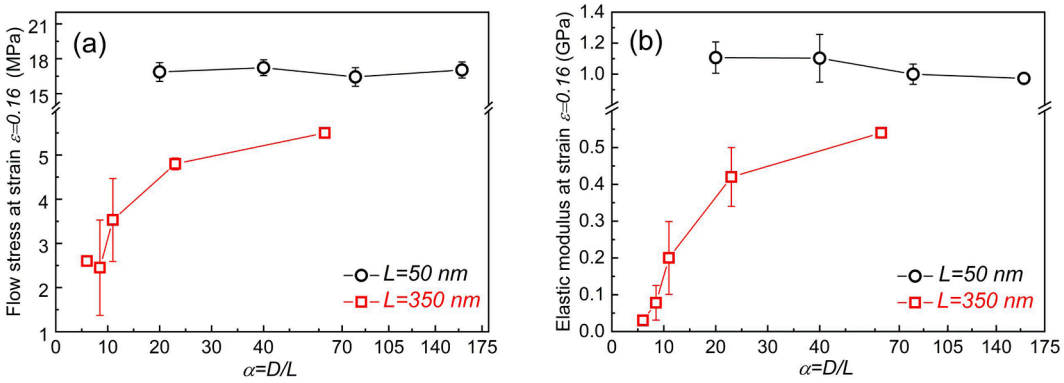

Fig. 4. (a) Flow stress and (b) elastic modulus at strain $\varepsilon = 0.16$ of pillars with varying ratio ($\alpha = D/L$) of pillar diameter (D) and ligament size (L). These data are captured from the stress–strain curves and elastic modulus of microcompression tests.

behavior. The flow stress of this coarse structure, displayed in Fig. 2 (c), is much lower than that of pillars with a small ligament size (50 nm), shown in Fig. 2 (a), owing to the size effect of "smaller is stronger". No distinct transition from elastic to plastic deformation is observed in the stress–strain curves shown in Fig. 2 (c), indicating that plastic deformation occurs immediately at the beginning of compression, in agreement with the macrocompression results presented in [15,23]. Furthermore, the reduction of α from 57 to 23 does not cause a great variation in flow stress, while a further reduction of α from 23 to 6 leads to a significant decrease in flow stress. It declines from 10 to 5 MPa at a strain of $\varepsilon = 0.27$ with decreasing α from 23 to 6, revealing a significant influence of deformation length scale (extrinsic size) on the mechanical response. Several drops were observed on the stress–strain curve of the pillar with $\alpha = 6$, implying the occurrence of non-uniform deformation and plasticity instability. The elastic modulus, plotted in Fig. 2 (d), exhibits the same trend as the flow stress. Here, the influence of α on the elastic modulus still can be inspected clearly on these curves, although the degree of noise on the measurement rises as α decreases. Comparing the SEM images of two pillars after compression, as shown in Fig. 2 (g) and (h), the pillar with $\alpha = 23$ ($D = 8$ μm) undergoes the expected uniform deformation dominated by uniaxial compression, while the other one with $\alpha = 6$ ($D = 2$ μm) seems to experience a mixed-mode deformation of torsion and compression. This discrepancy might be due to structural heterogeneity.

In order to further address this interesting behavior coming from such small structures with low α, we go into more detail on the stress–strain curves and the SEM images of pillars with $\alpha = 8.5$ ($D = 3$ μm, $L = 350$ nm) and $\alpha = 6$ ($D = 2$ μm, $L = 350$ nm), as displayed in Fig. 3 (a). Stochastic behavior of flow stress is found for the pillar with $\alpha = 8.5$, where the flow stress of one of the pillars is extremely lower than that of the others, and it keeps a quite low state until the strain reaches 0.23. However, no significant discrepancy in the structure is found from the SEM images displayed in Fig. 3 (c) of two pillars showing very different flow stress responses. This can be explained. The position of each pillar cut out of the polycrystalline NPG is selected randomly. Although all pillars are fabricated from the same bulk sample, there can be differences in local geometry or crystallographic orientation among the pillars. The most likely explanation for the observed extreme differences in plastic behavior of the different pillars with identical ligament size and pillar size lies in the location and connection of the only few load-bearing units which govern the mechanical response. As described in the following paragraph, this behavior becomes more distinctive if α is further reduced.

Consequently, more distinct non-uniform deformation was found when α is around 6. Although their α is identical, the pillars shown in Fig. 3 (b) exhibit totally different responses to the external load. The corresponding stress–strain curves reveal that the flow stress of one of the pillars is more than two times as high as the flow stress of the others and even higher than the flow stress of a pillar with larger $\alpha = 8.5$ shown in Fig. 3 (a). Interestingly, from the SEM images of pillars after compression, displayed in Fig. 3 (d), it is seen that the load-bearing units (i.e. the closed rings consisting of interconnected ligaments contributing to mechanical properties) of one of the pillars are incomplete. This suggests that the size of the load-bearing units is close to 6 times the corresponding ligament size.

4. Discussion

Our microcompression results indicate that both ligament size (L) and pillar diameter (D) have a significant influence on the elastic and plastic behavior of NPG within certain ranges. Structure coarsening from 50 to 350 nm will induce a considerable decrease in both strength and elastic modulus, consistent with the results in other studies [15,24,25]. In [26] a collection of compressive strength values for similar samples can be found. The two microstructural sizes investigated in this study show very good agreement if the value of α is high.

Based on the stress–strain curves of pillars with varying α, the flow stress and elastic modulus of pillars at strain $\varepsilon = 0.16$ as a function of $\alpha = D/L$ is summarized in Fig. 4. Apparently, both flow stress and elastic modulus exhibit the similar trend in the range of α from 160 to 6. They stay nearly constant for a fixed ligament size when α of the pillar is larger than 20. The flow stress is around 17 MPa for $L = 50$ nm and 5.5 MPa for $L = 350$ nm, while the elastic modulus remains ~ 1.1 and 0.5 GPa, respectively. Conversely, for the pillars with α lower than 20, where the

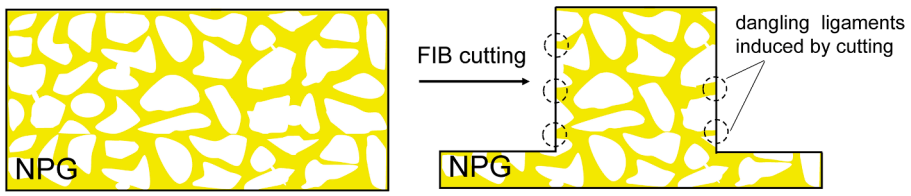

Fig. 5. Schematic of a pillar cut from a bulk NPG sample by FIB milling, where some ligaments at the wall side change from the interconnected to the dangling state caused by cutting.

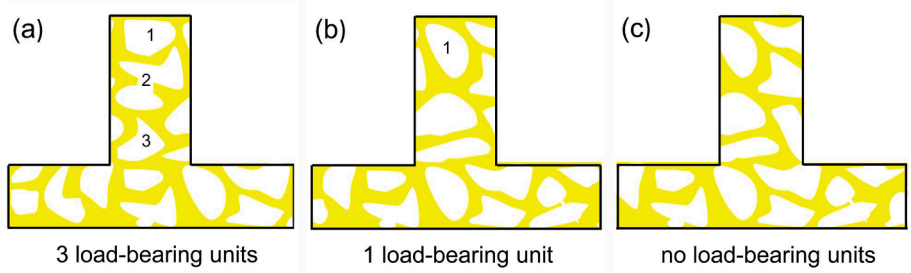

Fig. 6. Schematics of NPG pillars with the same α but different number of load-bearing units; (a) 3, (b) 1 and (c) without complete load-bearing units (closed load-bearing rings).

corresponding ligament size is 350 nm, reducing α leads to a significant decrease in both flow stress and elastic modulus. In addition, stochastic behavior and non-uniform deformation were found in pillars with $\alpha<10$. The basis for these size effects can be explained in terms of the reduction of connectivity and ligament size distribution, as will now be discussed.

Cutting a pillar of finite size out of the monolithic NPG sample will cause a change in the constraints of the ligaments at the column sidewall, as shown in Fig. 5, which causes an increase in the number of isolated and dangling ligaments. Thus, the number of non-interconnected ligaments that do not contribute to the connectivity and mechanical properties [27,28] relative to the accessible total number of ligaments increases with decreasing α, resulting in a reduction of the amount of the load-bearing units which might be considered as closed rings of interconnected ligaments. In the case of the pillars with sufficiently high α, the amount of connectivity reduction induced by cutting open closed rings at the side walls is small compared to the total number of closed rings, hence no influence of pillar diameter on the mechanical behavior can be discerned, as shown in Fig. 2(a) and (b). Yet, a change can be observed when α drops below 20. Concretely, both strength and elastic modulus of NPG with $L = 350$ nm decrease considerably with decreasing α from 23 to 6. This size effect is opposite from the conventional size effect of "smaller is stronger" found for massive metals [6] that is associated with dislocation interaction, movement, and/or nucleation during deformation. Our results show the importance of the connectivity between the ligaments in determination of elastic and plastic properties of nanoporous materials.

Further reduction of the pillar size, e.g. $\alpha < 10$, might produce the samples with few or even no complete load-bearing units, as shown in Fig. 6. This also can cause an increase of anisotropy in the structure. As a consequence, any failure of the local structure at the weakest load-bearing units dominates the response to the external load, resulting in stochastic behavior or even mechanical instability, as proven by stress–strain curves and SEM images of pillars with $\alpha = 8.5$ and 6 shown in Fig. 4. Additionally, according to the results of the structure analysis on NPG in [17], the distribution of ligament sizes of the bulk sample fabricated by electrochemical dealloying is broad, implying that the average ligament size of pillars with such low α might be different from each other, even though they are cut from the same bulk sample. This could be another factor leading to the irregular mechanical behavior since the deformation behavior is found to be highly dependent on the ligament size.

Based on our results and their discussion above, a critical ratio of $\alpha = 20$ was determined, above which the test structure can be considered a representative volume element (RVE) of bulk NPG resulting in a reproducible and uniform mechanical response. When α is lower than 20, the compression results of pillars with coarse structure ($L = 350$ nm) reveal that the flow stress and elastic modulus decrease with decreasing diameter of the pillars. A stochastic behavior is observed along with non-uniform deformation and failure when α decreases below 10. This size-dependent strength of NPG pillars found here is consistent with the corresponding compression results of Al foams [8,10]. However, due to the structural discrepancy between Al foams with elongated millimeter-scaled cells and NPG with random and nanoscaled ligaments, the size of the critical ratio ($\alpha = 20$) of the RVE found here is different from the size of the corresponding ratio ($\alpha = 8$) for the Al foam. Furthermore, the ratio ($\alpha = 15$) of the RVE for NPG identified by Hu *et al.* in [17] is a bit smaller than the value found in the current work, which might be attributed to the different ways of characterization. The RVE defined in [17], as the minimum size above which a set of structural parameters showed minimum variation, is based on the quantification analysis of structural parameters of NPG. Of course, this value holds only for those parameters and does not ensure that the mechanical behavior is reproducible. Here, the minimum ratio for obtaining an RVE is determined via analysis of the results of the mechanical response and structural morphology of the tested pillars.

5. Conclusion

In the current study, the consequence of microstructural length-scale and deformation length-scale effects in the mechanical behavior of NPG was investigated via microcompression testing on micro-pillars with varying ratio ($\alpha = D/L$) of pillar diameter (D) to ligament size (L). It was found that ligament coarsening can cause a significant decrease in flow stress and elastic modulus. For NPG with a fixed ligament size, the mechanical response shows independence on the sample size, here the diameter of the tested pillar, if α is larger than 20, while both flow stress and elastic modulus decrease with decreasing α if it is below 20. Based on these findings, a critical size ratio of $\alpha = 20$ is defined here, above which the test structure can be considered an RVE of NPG resulting in identical mechanical behavior and uniform deformation. For smaller size ratios α between 20 and 10, a decrease in mechanical stiffness and strength is caused by the increase in the relative number of non-connected parts of the ligament network. Furthermore, stochastic behavior along with non-uniform deformation and failure controlled by the local structure were observed when α decreases below 10, suggesting that the size of the load-bearing units in NPG is close to 10 times the ligament size.

Declaration of Competing Interest

The authors declare that they have no known competing financial interests or personal relationships that could have appeared to influence the work reported in this paper.

Data availability

The raw data required to reproduce these findings are available to download from doi:10.17632/7272jks75v.1

Acknowledgements

This work was supported by the Deutsche Forschungsgemeinschaft (DFG, German Research Foundation) – Project Number 192346071 – SFB 986 "Tailor-Made Multi-Scale Materials Systems: M^3".

References

[1] Z. Qi, J. Weissmüller, Hierarchical Nested-Network Nanostructure by Dealloying, ACS Nano 7 (7) (2013) 5948–5954.
[2] S. Shi, Y. Li, B.-N. Ngo-Dinh, J. Markmann, J. Weissmüller, Scaling behavior of stiffness and strength of hierarchical network nanomaterials, Science 371 (6533) (2021) 1026–1033.
[3] C. Volkert, E. Lilleodden, D. Kramer, J. Weissmüller, Approaching the theoretical strength in nanoporous Au, Appl. Phys. Lett. 89(6) (2006) 061920.
[4] M.D. Uchic, D.M. Dimiduk, J.N. Florando, W.D. Nix, Sample Dimensions Influence Strength and Crystal Plasticity, Science 305 (5686) (2004) 986–989.
[5] J.R. Greer, W.C. Oliver, W.D. Nix, Size dependence of mechanical properties of gold at the micron scale in the absence of strain gradients, Acta Mater. 53 (6) (2005) 1821–1830.
[6] C.A. Volkert, E.T. Lilleodden, Size effects in the deformation of sub-micron Au columns, Phil. Mag. 86 (33–35) (2006) 5567–5579.
[7] P.R. Onck, Scale Effects in Cellular Metals, MRS Bull. 28 (4) (2003) 279–283.
[8] P.R. Onck, E.W. Andrews, L.J. Gibson, Size effects in ductile cellular solids Part I: modeling, Int. J. Mech. Sci. 43 (3) (2001) 681–699.
[9] A.F. Bastawros, H. Bart-Smith, A.G. Evans, Experimental analysis of deformation mechanisms in a closed-cell aluminum alloy foam, J. Mech. Phys. Solids 48 (2) (2000) 301–322.
[10] E.W. Andrews, G. Gioux, P. Onck, L.J. Gibson, Size effects in ductile cellular solids. Part II: experimental results, Int. J. Mech. Sci. 43 (3) (2001) 701–713.
[11] R. Brezny, D.J. Green, Characterization of edge effects in cellular materials, J. Mater. Sci. 25 (11) (1990) 4571–4578.
[12] I.J. Gibson, M.F. Ashby, The mechanics of three-dimensional cellular materials, Proceedings of the Royal Society of London. A. Mathematical and Physical Sciences 382(1782) (1982) 43-59.
[13] J. Li, Y. Zhang, C. Tian, H. Zhou, G. Hu, R. Xia, Structurally ordered nanoporous Pt–Co alloys with enhanced mechanical behaviors in tension, Microporous Mesoporous Mater. 295 (2020), 109955.
[14] Y. Zhang, J. Li, Y. Hu, S. Ding, F. Du, R. Xia, Characterization of the deformation behaviors under uniaxial stress for bicontinuous nanoporous amorphous alloys, PCCP 24 (2) (2022) 1099–1112.
[15] N. Mameka, K. Wang, J. Markmann, E.T. Lilleodden, J. Weissmüller, Nanoporous Gold—Testing Macro-scale Samples to Probe Small-scale Mechanical Behavior, Mater. Res. Lett. 4 (1) (2016) 27–36.
[16] K.R. Mangipudi, E. Epler, C.A. Volkert, Topology-dependent scaling laws for the stiffness and strength of nanoporous gold, Acta Mater. 119 (2016) 115–122.
[17] K. Hu, M. Ziehmer, K. Wang, E.T. Lilleodden, Nanoporous gold: 3D structural analyses of representative volumes and their implications on scaling relations of mechanical behaviour, Phil. Mag. 96 (32–34) (2016) 3322–3335.
[18] J. Jiao, N. Huber, Deformation mechanisms in nanoporous metals: Effect of ligament shape and disorder, Comput. Mater. Sci 127 (2017) 194–203.
[19] B. Zandersons, L. Lührs, Y. Li, J. Weissmüller, On factors defining the mechanical behavior of nanoporous gold, Acta Mater. 215 (2021), 116979.
[20] Y. Li, B.-N. Dinh Ngô, J. Markmann, J. Weissmüller, Topology evolution during coarsening of nanoscale metal network structures, Phys. Rev. Mater. 3 (7) (2019), 076001.
[21] Y. Wu, J. Markmann, E.T. Lilleodden, Electro-chemo-mechanical coupling of nanoporous gold at the microscale, Appl. Phys. Lett. 115(25) (2019) 251602.
[22] I.N. Sneddon, The relation between load and penetration in the axisymmetric boussinesq problem for a punch of arbitrary profile, Int. J. Eng. Sci. 3 (1) (1965) 47–57.
[23] B.-N.-D. Ngô, A. Stukowski, N. Mameka, J. Markmann, K. Albe, J. Weissmüller, Anomalous compliance and early yielding of nanoporous gold, Acta Mater. 93 (2015) 144–155.
[24] J. Biener, A.M. Hodge, J.R. Hayes, C.A. Volkert, L.A. Zepeda-Ruiz, A.V. Hamza, F. F. Abraham, Size Effects on the Mechanical Behavior of Nanoporous Au, Nano Lett. 6 (10) (2006) 2379–2382.
[25] N. Badwe, X. Chen, K. Sieradzki, Mechanical properties of nanoporous gold in tension, Acta Mater. 129 (2017) 251–258.
[26] Y.-Y. Zhang, L. Zou, L.-Z. Liu, H. Xie, C.-H. Li, H.-J. Jin, Mechanical properties of unidirectional nanoporous gold under compression, Acta Mater. 235 (2022), 118078.
[27] L.-Z. Liu, H.-J. Jin, Scaling equation for the elastic modulus of nanoporous gold with “fixed” network connectivity, Appl. Phys. Lett. 110(21) (2017) 211902.
[28] L.-Z. Liu, X.-L. Ye, H.-J. Jin, Interpreting anomalous low-strength and low-stiffness of nanoporous gold: Quantification of network connectivity, Acta Mater. 118 (2016) 77–87.